# Substituent Effect on Electrochemical and Electrochromic Behaviors of Ambipolar Aromatic Polyimides Based on Aniline Derivatives

Li-Ting Huang, Hung-Ju Yen, and Guey-Sheng Liou*

Functional Polymeric Materials Laboratory, Institute of Polymer Science and Engineering, National Taiwan University, 1 Roosevelt Road, 4th Sec., Taipei 10617, Taiwan

S *Supporting Information*

ABSTRACT: Three series of new ambipolar polyimides containing aniline derivatives with different degree of 4-methoxyphenyl substituent showing anodically/cathodically electrochromic characteristic were prepared from the polycondensation of three diamine monomers—4,4′-bis[(4-aminophenyl)amino]diphenylamine (**3**), 4,4′-bis[(4-aminophenyl)amino]-4″-methoxytriphenylamine (**3′**), and 4,4′-bis[4-aminophenyl(4-methoxyphenyl)amino]-4″-methoxytriphenylamine (**3″**)—with various commercially available tetracarboxylic dianhydrides. In addition to the high glass-transition temperatures (T_g, 246−339 °C), thermal stability, and solution processability, the resulting polyimide films exhibited ambipolar electrochromic behavior. The nonconjugated TPA-based polyimides **III** revealed more stable electrochemical oxidation behavior and better electrochromic reversibility than conjugated DPA-based corresponding polyimides **I** due to the additional phenyl ring providing the route to stabilize the cation radical formed during oxidation.

Triphenylamine-Substituted Derivative Polyimides

Ambipolar Multi-Electrochromism
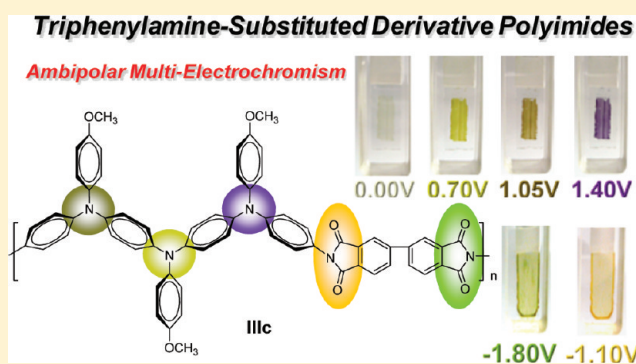
■ INTRODUCTION

Electrochromic (EC) materials exhibit a reversible optical change in absorption or transmittance upon electrochemically oxidized or reduced; the EC effect has been known for quite some time, and great strides have been made with transition-metal oxides (e.g., WO_3), inorganic coordinating complexes, organic molecules, and electrodeposited π-conjugated polymers films.[1] Among the conjugated polymers, polyaniline (PANI) has long been considered a strong contender in the field of polymer electronics due to its variable color changes depending on the redox state, and its electrical properties can be modified by p-doping (i.e., changing the oxidation state) or by acid−base chemistry (affecting the protonation states).[2] However, PANI could not provide detailed understanding of the relation between the structural disorder and the electronic transport. For this reason, oligoanilines with similar but clearly defined molecular structures compared to polymers have attracted much attention as theoretical models and also could exhibit new properties or even find new application.[3] Similar to other conjugated polymers, the structural configuration and chain length of polymers have a great effect on the optical and physical properties, such as the oxidation potential of oligoanilines decreasing with increasing their chain length.[4] Recently, the electroactive polymers with aniline oligomer have been widely studied, such as polyamide,[5] polyimide,[6] epoxy,[7] dendrimer,[8] and others.[9] There have been significant works published on these π-conjugated polymers focused on their electrochemical behaviors and electrochromic properties; in essence, these polymers could switch between two or more different color states. Nevertheless, the long-term stability of these aniline-derivative polymers was rarely investigated due to the switching time might be elongated after cyclic scans and the environmental instability.[10] In addition, the major drawbacks of all the different classes of π-conjugated polymers are the issues of poor solubility, low processability, and difficulty of switching from one distinct color of neutral state to a highly transmissive and near colorless of oxidative state,[11] which largely limits the influence on the demanding of highly transparent and colorless EC windows without any applied potential at neutral state in applications.

For organic electroactive triphenylamine (TPA) materials, the characteristic structure feature of TPA is the electroactive site of the nitrogen center, which is linked to three electron-rich phenyl groups in a propeller-like geometry. The anodic oxidation behavior of TPA has been well studied.[12] The electrogenerated cation radical of TPA•+ is not stable and could form tetraphenylbenzidine (TPB) by tail-to-tail coupling. When the phenyl groups were incorporated by electron-donating substituents at the para position of TPA, the coupling reactions could be greatly prevented by affording stable cationic radicals.[13] Intramolecular electron transfer (ET) processes were also investigated extensively in the mixed-valence (MV) systems[14] and usually employed one-dimensional MV compounds contain two or more redox states connected via π-bridge molecule. According

to Robin and Day,[15] the cation radical has been reported as a symmetrical delocalized class III structure with a strong electronic coupling (the electron is delocalized over the two or more redox centers), leading an intervalence charge transfer (IV-CT) absorption band in the NIR region.[16] Since 2005, our group has reported several TPA-containing electrochromic polymers with interesting multicolor transitions[17] that showed good electrochromic reversibility in the visible region and NIR range. Compared with the electrochromic π-conjugated polymers, the nonconjugated TPA-based polymers exhibited highly transmissive in the neutral state and multicolor in the oxidized states. In this article, in order to investigate electrochemical and electrochromic behaviors of the structurally related TPA-based polymers and aniline-based polymers, we therefore synthesized a novel diamine monomer, 4,4′-bis[(4-aminophenyl)amino]-4″-methoxytriphenylamine (3′) containing one 4-methoxyphenyl substituted tertiary amino and two secondary amino moieties and their corresponding aromatic polyimides. For comparison, the structurally related two series of polyimides were also prepared from the diamines 4,4′-bis[(4-aminophenyl)amino]-diphenylamine (3) with structure close to PANI and 4,4′-bis-[4-aminophenyl(4-methoxyphenyl)amino]-4″-methoxytriphenylamine (3″).[18]


3

3'

3"
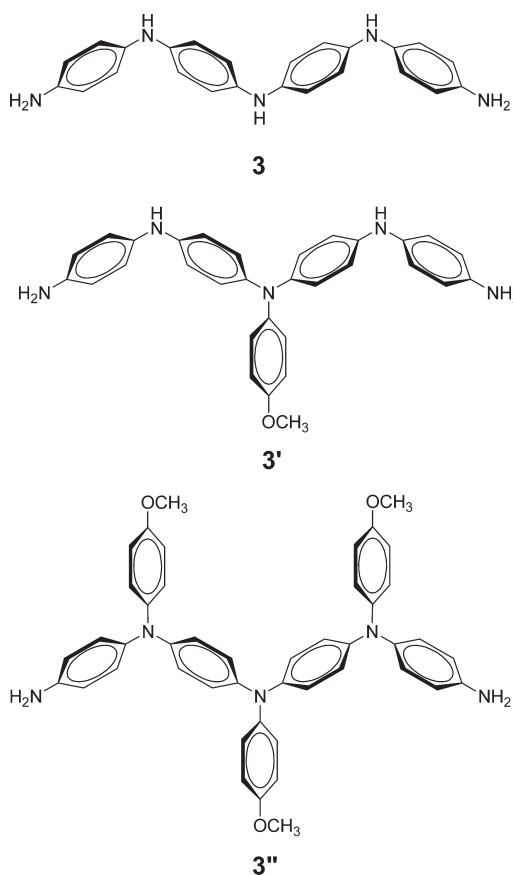
■ RESULTS AND DISCUSSION

Monomer Synthesis. 4,4′-Bis[(4-aminophenyl)amino]diphenylamine (3) was prepared by the triethylamine-mediated aromatic nucleophilic substitution reaction of 4,4′-diaminodiphenylamine

with 4-fluoronitrobenzene followed by hydrogen Pd/C-catalyzed reduction according to the synthetic route outline in Scheme 1. The new monomer 4,4′-bis[(4-aminophenyl)amino]-4″-methoxytriphenylamine (3′) was synthesized by hydrogen Pd/C-catalyzed reduction of the dinitro compound 4,4′-bis-[(4-nitrophenyl)amino]-4″-methoxytriphenylamine (2′) resulting from the triethylamine-mediated aromatic nucleophilic substitution reaction of 4,4′-diamino-4″-methoxytriphenylamine with 4-fluoronitrobenzene (Scheme 1). Synthesis and characterization data of compounds 4,4′-bis[(4-nitrophenyl)amino]diphenylamine (2), 4,4′-bis[(4-aminophenyl)amino]diphenylamine (3), 4,4′-bis[(4-nitrophenyl)amino]-4″-methoxytriphenylamine (2′), and 4,4′-bis[(4-aminophenyl)amino]-4″-methoxytriphenylamine (3′) were included in the Supporting Information (Figures S1−S4) and also agreed well with the proposed molecular structures.

Polymer Synthesis. Two series of polyimides I and II were prepared by the polycondensation of diamines 3 and 3′ with two commercially available dianhydrides 4a and 4b via a conventional two-step process (as shown in Scheme 2), respectively. In the first step, the reaction mixtures became very viscous, indicating the formation of poly(amic acid)s with high molecular weight. The poly(amic acid) precursors could be chemically dehydrated to the corresponding polyimides by treatment with acetic anhydride and pyridine. Because of no secondary amine group within monomer diamine 3″, the series of polyimides III could be prepared readily by one-step polymerization of diamine 3″ and dianhydrides 4 in m-cresol at 185 °C in the presence of isoquinoline as the catalyst. These obtained polyimides had inherent viscosities in the range of 0.33−1.34 dL/g with weight-average molecular weights (M_w) and polydispersity (PDI) of 57 000−143 000 Da and 1.54−2.35, respectively, relative to polystyrene standards (Table S1). All polyimides could afford tough and free-standing films. The formation of polyimides was confirmed by IR and NMR spectroscopy (as shown in Figures S5−S7). The IR spectra of polyimides (Ia−IIIa) exhibited characteristic imide absorption bands at around 1781 (symmetrical C=O), 1720 (symmetrical C=O), 1380 (C−N), and 738 cm^{-1} (imide ring deformation). The structures of these polyimides were also verified by NMR spectra, and Figure S6 shows a typical set of ^{1}H and ^{13}C NMR spectra of polyimides IIa in DMSO-d_6; all the peaks could be readily assigned to the hydrogen and carbon atoms of the recurring unit. No resonance peak appeared around 10 ppm in the ^{1}H NMR spectrum support the completed imidization. Assignments of each carbon and proton were assisted by the two-dimensional H−H COSY and C−H HSQC NMR spectra shown in Figure S7 and agree well with the proposed molecular structure of IIa.

Solubility. The solubility properties of polyimides I−III in some organic solvent were investigated qualitatively, and the results are summarized in Table S2 of the Supporting Information. The solubility behavior of these polyimides depends on their chain packing and intermolecular interaction affected by the rigidity, symmetry, and regularity of the molecular backbone. Polyimides III derived from diamine with higher steric hindrance and bulky phenyl groups showed higher solubility not only in polar aprotic organic solvents such as NMP, DMAc, and m-cresol but also in less polar solvents like THF and CHCl₃. Because of the strong hydrogen-bonding interaction and less steric hindrance for close packing, the polymers I exhibited the lowest solubility among all the three series of polyimides. The polyimides I−III obtained from

Scheme 1. Synthetic Routes to Diamine Compounds 3 and 3′
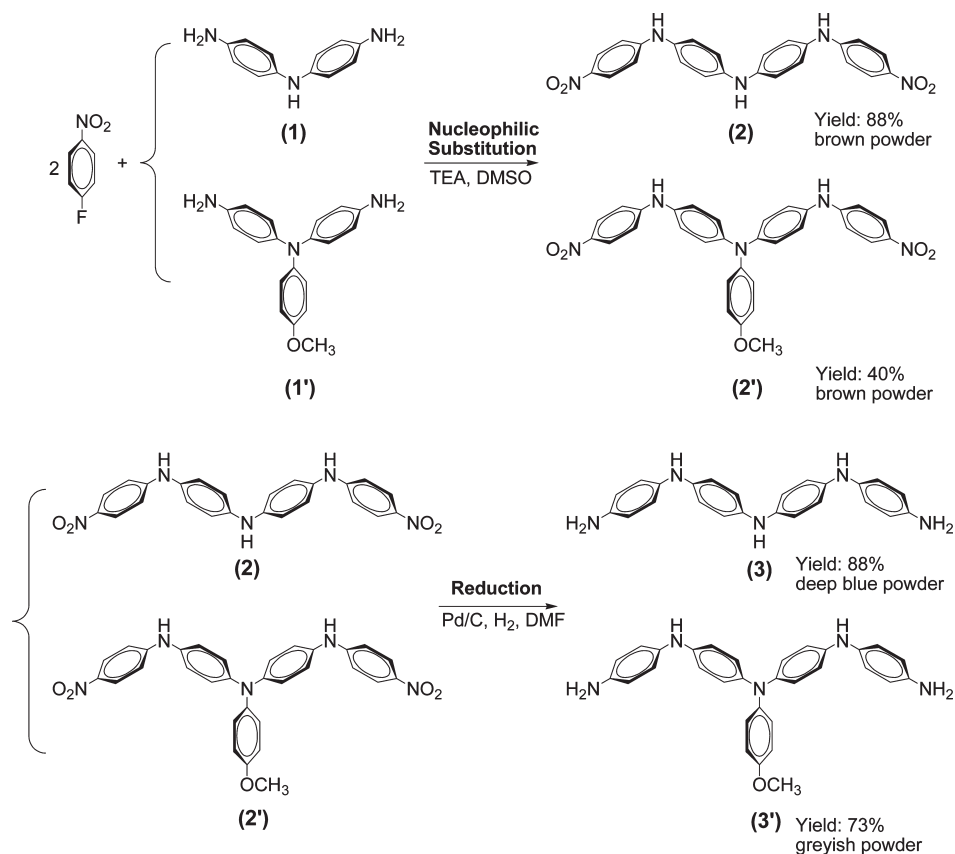
Scheme 2. Synthesis and Structures of Polyimides I−III
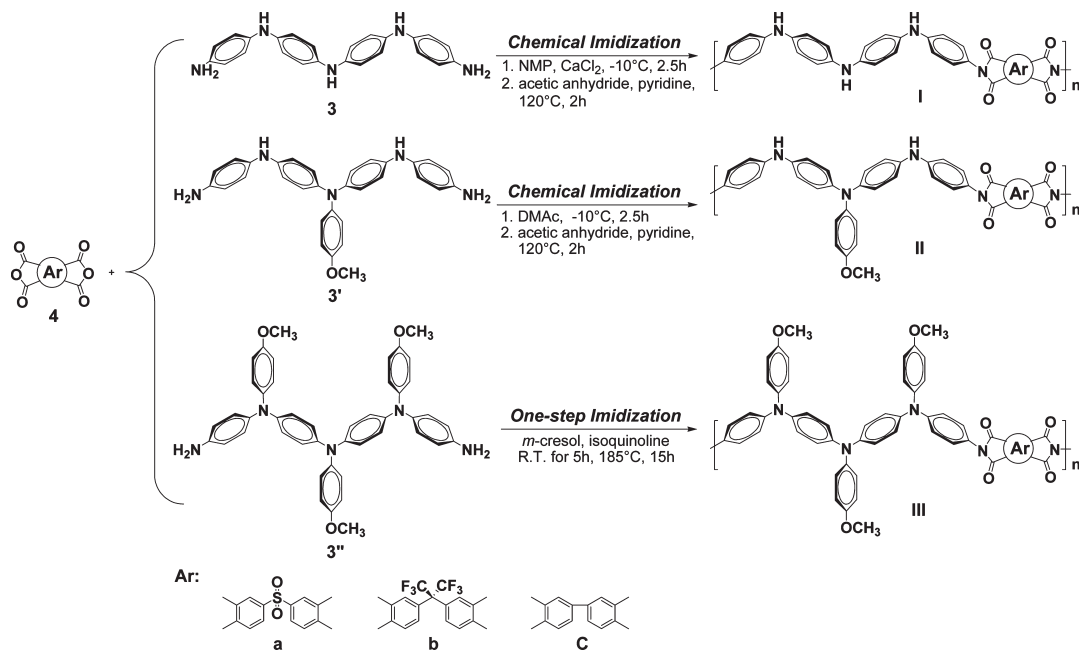
dianhydride **4b** revealed better solubility than those of prepared from **4a** because of the additional contribution of the hexafluoroisopropylidene ($-C(CF_3)_2-$) group in the polymer backbone

which reduce the intermolecular interactions and close packing. Thus, the excellent solubility makes these polymers as potential candidates for practical applications by spin-coating or
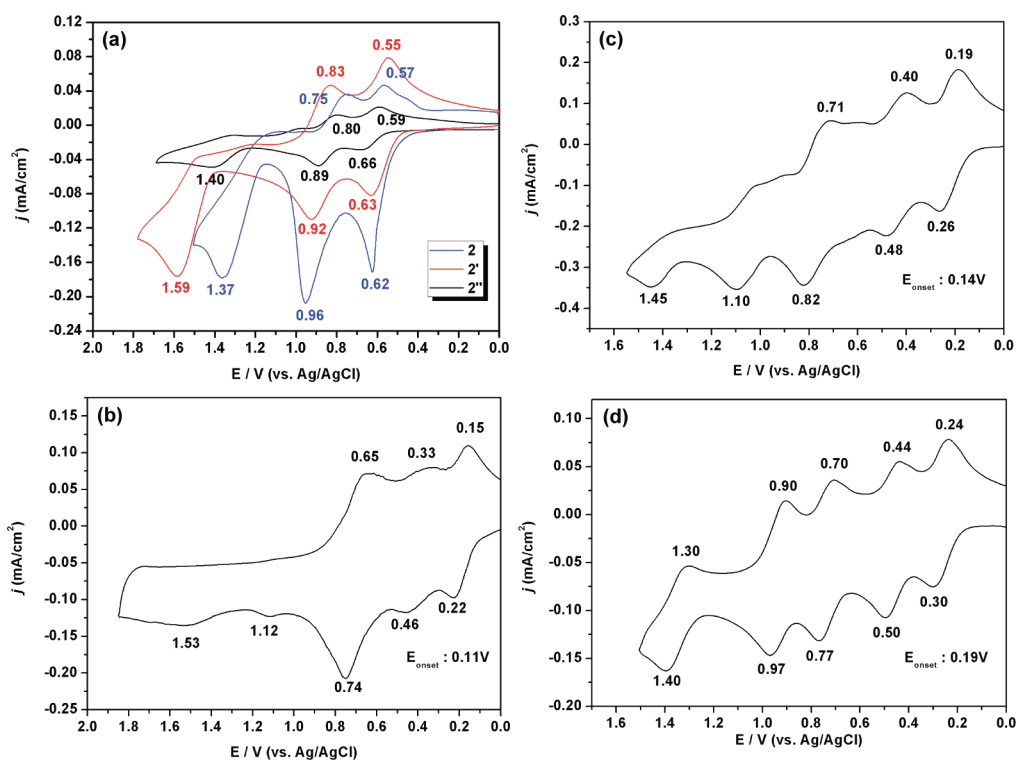
Figure 1. Cyclic voltammograms of 10^{-3} M (a) dinitro compounds **2**, **2′**, and **2″** and diamino compounds (b) **3**, (c) **3′**, and (d) **3″** in CH$_3$CN containing 0.1 M TBAP. Scan rate = 50 mV/s.

Table 1. Redox Potentials and Energy Levels of Compounds

| code | oxidation (V) (vs Ag/AgCl) | | | | | | λ_{onset} (nm) | HOMO[b] | LUMO[c] | $E_g{}^d$ |
	E_{onset}	$E_{1/2(ox,1)}$	$E_{1/2(ox,2)}$	$E_{1/2(ox,3)}$	$E_{1/2(ox,4)}$	$E_{1/2(ox,5)}$				
2	0.49	0.60	0.86	1.37[a]			532	4.96	2.63	2.33
2′	0.48	0.59	0.88	1.59[a]			535	4.93	2.61	2.32
2″	0.54	0.63	0.85	1.40[a]			528	4.99	2.64	2.35
3	0.11	0.19	0.40	0.70	1.15[a]	1.53[a]		4.55		
3′	0.14	0.23	0.44	0.77	1.10[a]	1.45[a]		4.59		
3″	0.19	0.27	0.47	0.74	0.94	1.35		4.63		

[a] Irreversible peak potential. [b] The HOMO energy levels were calculated from cyclic voltammetry and were referenced to ferrocene (4.8 eV, $E_{1/2}$ = 0.44 V). [c] LUMO = HOMO − E_g. [d] E_g = 1240/λ_{onset}.

inkjet-printing processes to afford high-performance thin films for optoelectronic devices.

Thermal Properties. The thermal properties of polyimides recorded by TGA and TMA are summarized in Table S3. Typical TGA curves of polyimides **Ia**, **IIa**, and **IIIa** are depicted in Figure S8. All the prepared polyimides exhibited good thermal stability with insignificant weight loss up to 350 °C under nitrogen or air atmosphere. The 10% weight loss temperatures of these polymers in nitrogen and air were recorded in the range of 460−630 and 450−585 °C, respectively. The amount of carbonized residue (char yield) of these polymers in nitrogen atmosphere was more than 58% at 800 °C. The high char yields of these polymers can be ascribed to their high aromatic content. The lowest T_d value of polyimide **I** series could be explained in terms of the less aromatic segment in its backbone. These polymers not only showed

good thermal stability but also possessed high glass-transition temperatures (T_g) in the range 246−339 °C. TMA curves of polyimides **Ia**, **IIa**, and **IIIa** are shown in Figure S9. The polyimide **I** series exhibited the higher T_g values that could be attributed to the strong interaction of hydrogen bonding between the secondary amine and carbonyl groups in the polymer chains. Besides, the sulfone type polyimides revealed the higher T_g due to their higher intermolecular force resulted from sulfone group which could provide strong dipole interactions relative to other connecting groups.

Electrochemical Properties. The electrochemical behavior of compounds **2**−**2″** and **3**−**3″** series and the polyimide **I**−**III** series was investigated by cyclic voltammetry (CV). Compounds were dissolved in dry acetonitrile (concentration 10^{-3} mol/L), and the polymers were conducted by cast film on an indium−tin oxide (ITO)-coated glass substrate as working electrode
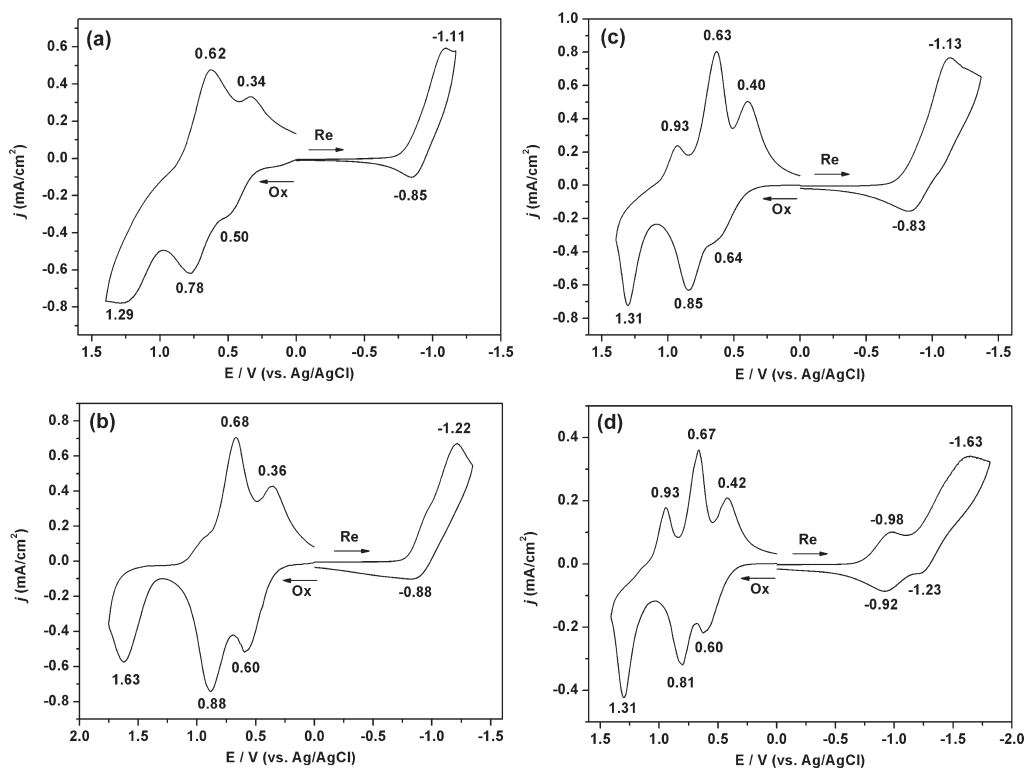
Figure 2. Cyclic voltammograms of the polyimide films (a) **Ia**, (b) **IIa**, (c) **IIIa**, and (d) **IIIc** on an ITO-coated glass substrate in 0.1 M TBAP acetonitrile (for anodic process) and DMF (for cathodic process) solution at a scan rate of 50 and 100 mV/s.
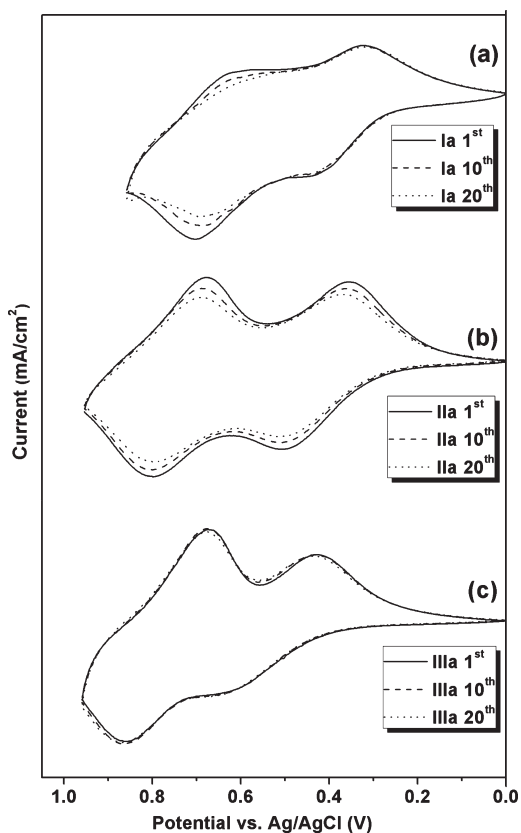

Figure 3. Cyclic voltammetric diagrams of polyimide (a) **Ia**, (b) **IIa**, and (c) **IIIa** films on an ITO-coated glass substrate over cyclic scans in 0.1 M TBAP/CH$_3$CN at a scan rate of 50 mV/s.

containing 0.1 M of tetrabutylammonium perchlorate (TBAP) as an electrolyte under a nitrogen atmosphere. The oxidation and reduction measurements of the polymer films were measured in acetonitrile (CH$_3$CN) and DMF, respectively. The typical CV diagrams for compounds **2**−**2″** and **3**−**3″** are depicted in Figure 1, and quantitative details are summarized in Table 1. There are three and five oxidation redox couples for compounds **2**−**2″** (Figure 1a) and monomers **3**−**3″**, respectively. As the substituent changed from electron-withdrawing nitro group to the electron-donating amino group, monomers **3**−**3″** exhibited lower oxidation potentials than those of compounds **2**−**2″**, indicating the inductive effect of the substituent on the oxidation reaction. Furthermore, replacing hydrogen atom by incorporation of methoxy-substituted phenyl groups into the electroactive nitrogen site of amino moieties resulted in increasing the applied potential values in the first oxidation stage, while these extra phenyl rings with electron-donating methoxy groups could provide routes for stabilizing the cation radical formed during oxidation procedure, thus enhancing the electrochemical reversibility. In the case of polymer system as shown in the Figure 2, all the polyimides underwent a three-stage one-electron oxidation originating from amine units, and only one-electron reduction induced by the aromatic-carbonyl π-system of the imide functional group could be observed from the imide ring of DSDA polyimides **Ia**−**IIIa** and 6FDA polyimides **Ib**−**IIIb**, indicating that the conjugation across the imide was interrupted by the sulfonyl and hexafluoroisopropylidene linkages. All the DSDA polyimides **Ia**−**IIIa** showed the lower reduction potential values than that of the 6FDA polyimides **Ib**−**IIIb**, implying that the sulfonyl bridge has more electron-withdrawing capability. The CV curve of BPDA polyimide **IIIc** (Figure 2d)

Table 2. Redox Potentials and Energy Levels of Polyimides

	thin films	oxidation[a]			reduction[b]						
code	λ_{onset}	E_{onset}	$E_{1/2(ox1)}$	$E_{1/2(ox2)}$	$E_{1/2(ox3)}$	E_{onset}	$E_{1/2(re1)}$	$E_{1/2(re2)}$	E_g^{opt}/eV[c]	E_g^{EC}/eV[d]	HOMO[e]	LUMO[e]
Ia	733	0.28	0.42	0.70	1.29[c]	−0.78	−0.98		1.69	1.48	4.78	3.30
Ib	727	0.27	0.40	0.68	1.22[c]	−1.02	−1.21		1.71	1.69	4.76	3.07
IIa	563	0.34	0.48	0.78	1.63[c]	−0.78	−1.05		2.20	1.61	4.84	3.23
IIb	560	0.33	0.46	0.78	1.43[c]	−1.04	−1.23		2.21	1.77	4.82	3.05
IIIa	560	0.40	0.52	0.74	1.12	−0.73	−0.98		2.21	1.58	4.88	3.30
IIIb	557	0.38	0.51	0.74	1.29[c]	−0.94	−1.20		2.23	1.79	4.87	3.08
IIIc	564	0.37	0.51	0.74	1.12	−0.69	−0.95	−1.43	2.20	1.54	4.87	3.33

[a] Versus Ag/AgCl in CH_3CN. $E_{1/2}$: average potential of the redox couple peaks. [b] Versus Ag/AgCl in DMF. [c] Bandgaps calculated from absorption edge of the polymer films: $E_g^{opt} = 1240/\lambda_{onset}$. [d] E_g^{EC}: electrochemical band gap is derived from the difference between the HOMO and LUMO levels. [e] The HOMO and LUMO energy levels were calculated from $E_{1/2ox}$ and $E_{1/2re}$ value of CV curves and were referenced to ferrocene (4.8 eV; $E_{1/2} = 0.44$ V in CH_3CN; $E_{1/2} = 0.52$ V in DMF).

exhibited two quasi-reversible one-electron reduction couples occurred at $E_{1/2} = -0.95$ and -1.43 V, corresponding to the formation of radical anion and dianions, respectively. Meanwhile, the first-stage reduction process occurred at a lower applied potential than polyimides **IIIa** and **IIIb**. The decreased reduction potential of polyimide **IIIc** could be attributed to the strong electron coupling between two phthalimide groups. This phenomenon could also be found in Kapton synthesized from 4,4′-oxidianiline (ODA) and pyromellitic dianhydride (PMDA) with two reduction couples at $E_{1/2} = -0.83$ and -1.34 V.[20] The difference between the first and second reduction process of Kapton from $E_{1/2}$ value (ΔE) was QJ;0.51 V, which was larger than polyimide **IIIc** ($\Delta E = 0.48$), revealing the PMDA segment possessed stronger electron transfer than BPDA.[14b] The continuous CV scanning was used to investigate the donor effect on the electrochemical stability (p-doping), and the results are depicted in Figure 3. Because the 4-methoxyphenyl group can stabilize the cation radicals, polyimide **IIIa** exhibited the best reversible CV behavior in the second oxidation stages. The redox potentials of the polyimides as well as their respective highest occupied molecular orbital (HOMO) and lowest unoccupied molecular orbital (LUMO) (versus vacuum) are calculated and summarized in Table 2.

Particularly, the electrochemical properties of structurally related polyaniline (PANI) had long been studied in the acidic solution.[21] In order to get more insight into the solvent effect on the mechanism of these structurally related polymers in this study, we therefore investigated the electrochemical behaviors of PANI in 1 M HCl and 0.1 M $TBAP/CH_3CN$ system, respectively. PANI films synthesized by electrochemical deposition were carried out using 0.1 M aniline in a solution of 0.5 M sulfuric acid at constant potential (0.9 V vs Ag/AgCl) for 6 min, the doped green PANI could be readily deposited onto working electrode and washed by water several times to remove aniline monomer, then dipped in 5 wt % $Na_2CO_{3(aq)}$ for 30 s (changing color from green to blue), and washed completely with water to remove salts. Finally, the dedoped blue PANI film was quickly dipped in acetone to remove water and dried under a nitrogen atmosphere. As the obtained PANI films were at fully oxidized state, we held on −0.2 V for 1 min before CV scanning. It is worth to note that the fully oxidized PANI film could not be reduced in nonacidic solution; thus, the acidic electrolytes were used before anodic scanning and washed by
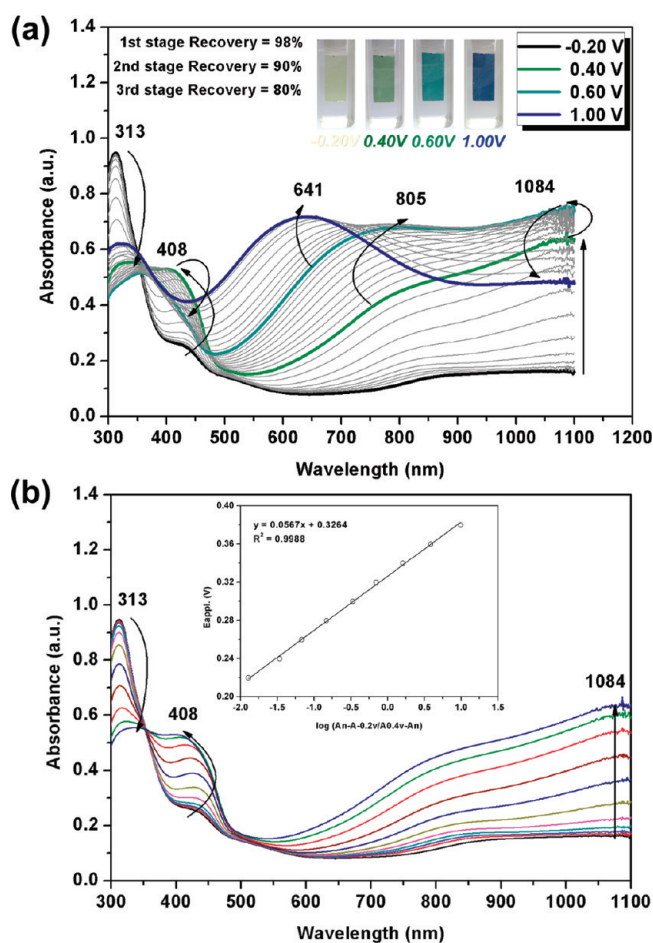

Figure 4. Absorption spectra change of the PANI films (∼750 nm in thickness) on the ITO-coated glass substrate (deposited area: 1.2 cm × 0.6 cm) in 1 M HCl at various applied potentials between (a) −0.20 and 1.00 and (b) −0.20 and 0.40 (V vs Ag/AgCl).

water to remove HCl. The electrochemical behaviors of PANI are shown in Figure S10, the CV diagrams of PANI in acid electrolytes revealed three reversible oxidation redox couples (Figure S10a), and the redox reaction for PANI is postulated in Scheme S1. The first and third oxidized stages associated with the oxidation of the electroactive nitrogen site.
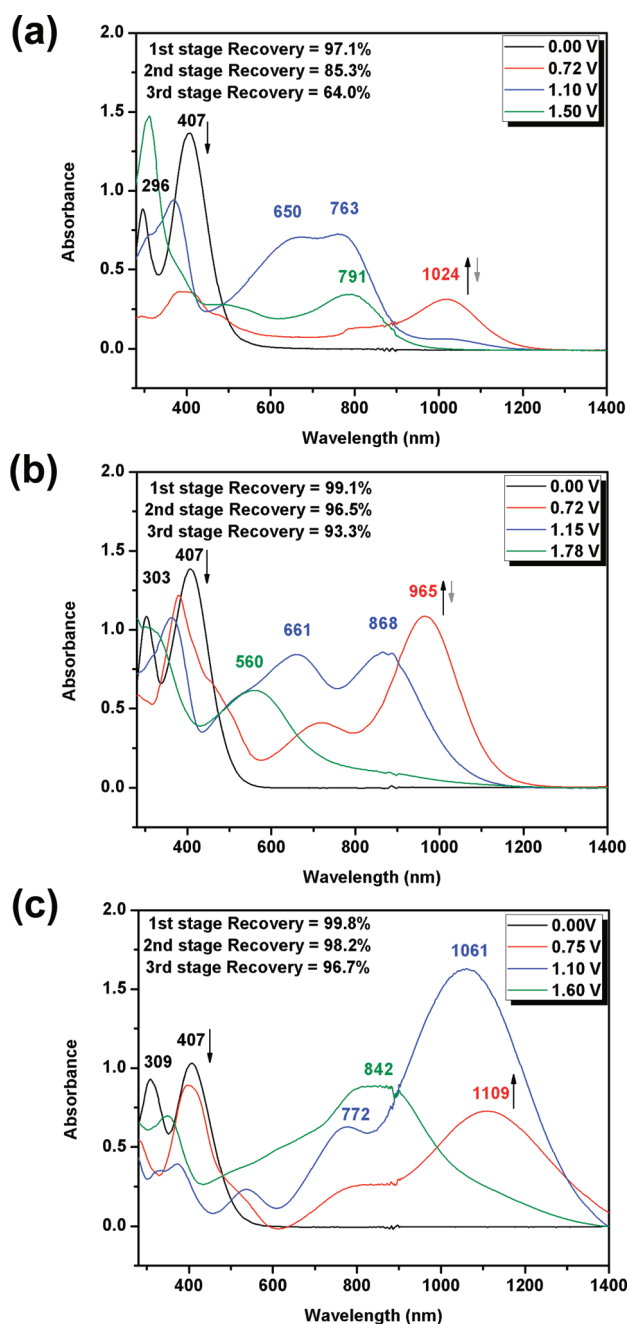
Figure 5. Absorption spectra of 5×10^{-4} M dinitro compounds (a) **2**, (b) **2′**, and (c) **2″** in CH$_3$CN solution containing 0.1 M TBAP at applied potentials of different oxidative stages (V vs Ag/AgCl).

The second redox couple ($E_{1/2} = 0.51$ V) in anodic scan could be attributed to the formation of quinones (mostly benzoquinone) as a consequence of hydrolysis in water. It has been reported that the loss of electrochemical response was accompanied by a large increased frequency, indicating the products formed by hydrolysis of the oxidized structures (changing imine into benzoquinone) were soluble.[21c] The PANI film gradually degraded while the potential was increased more than 0.85 V and lost its electrochemical properties after continuous 10 cyclic scans both in the acidic and nonacidic systems (Figure S10). The latter system exhibited

lower reversibility due to the stable imine (C=N) structure could not be reduced by regaining protons from nonacidic electrolytes.

Measurement of *n* Electrons Transfered for PANI. Polyaniline was known as its color changes depending on the redox states. However, some results reported previously described the PANI oxidation processes losing two electrons and protons in each oxidized states.[21c] In order to confirm the mechanism of how many electrons *n* were transferred for each step by the OTTLE techniques, a series of potentials, E_{applied}, were sequentially impressed (potentiostated) across the transparent cell containing a PANI film of the redox couple. At each applied potential, the ratio of the concentrations of oxidized to neutral forms [O]/[N] of the couple adjusted by electrolysis at the transparent electrode to the value required for adherence to the Nernst equation:[12,22]

$$ \text{O} + n\text{e}^- + m\text{H}^+ \leftrightarrow \text{R} $$

$$ E_{\text{applied}} = \left(E_0 + \frac{0.059}{n} \ln \frac{[\text{O}]}{[\text{R}]} \right) - 0.059 \frac{m}{n} \text{pH} $$

where *n* represents the number of reacting electrons and *m* represents the number of reacting protons. However, the oxidation potential for this reaction was independent of pH because of the pH value was zero in 1 M HCl. For the reaction, the Nernst equation is

$$ E_{\text{applied}} = E_0 + \frac{0.059}{n} \log \left(\frac{[\text{O}]}{[\text{N}]} \right) $$

where E_{applied} and E_0 represent the actual and standard potentials, respectively, O and N represent the oxidized and neutral species, and 0.059 represents the ratio of the gas constant to the Faraday constant at room temperature. The [O]/[N] value corresponding to each E_{applied} to be obtained from absorbance changes measured by recording spectra after equilibrium is achieved for each potential.

Figure 4a shows the optical absorption and color changes for PANI at various applied potentials in 1 M HCl. The absorption peaks at 313 and 408 nm are characteristic for PANI. After one-electron oxidation (-0.20 to 0.40 V), the original peak at 313 nm decreased and the 408 nm and a broad band at around 1084 nm increased gradually. The first oxidation reversibility was 98% based on the absorbance at 313 nm. When the potential was adjusted to more positive values (0.40–0.60 V) corresponding to the second stage oxidation, the characteristic new peaks appeared at 805 and 1084 nm increased with the decreasing at 408 nm, and the second oxidation reversibility was 90%. For the third oxidative state (0.60–1.00 V), the peak at 1084 nm decreased obviously with a reversibility of only 80%, implying the lower stability of this product at third oxidation stage. The PANI film switches from a pale yellowish neutral state to the green/bluish green and then blue oxidized states. The inset curve in Figure 4b shows a typical plot of E_{applied} vs $\log(A_n - A_0)/(A_f - A_n)$ corresponding to 1084 nm (IV-CT band) for the first coloring stage. The slope of the straight-line plot is 56.7 mV, which compares

Scheme 3. Postulated Redox Behavior of the Dinitro Compounds 2, 2′, and 2″

dx.doi.org/10.1021/ma202128e |*Macromolecules* 2011, 44, 9595–9610
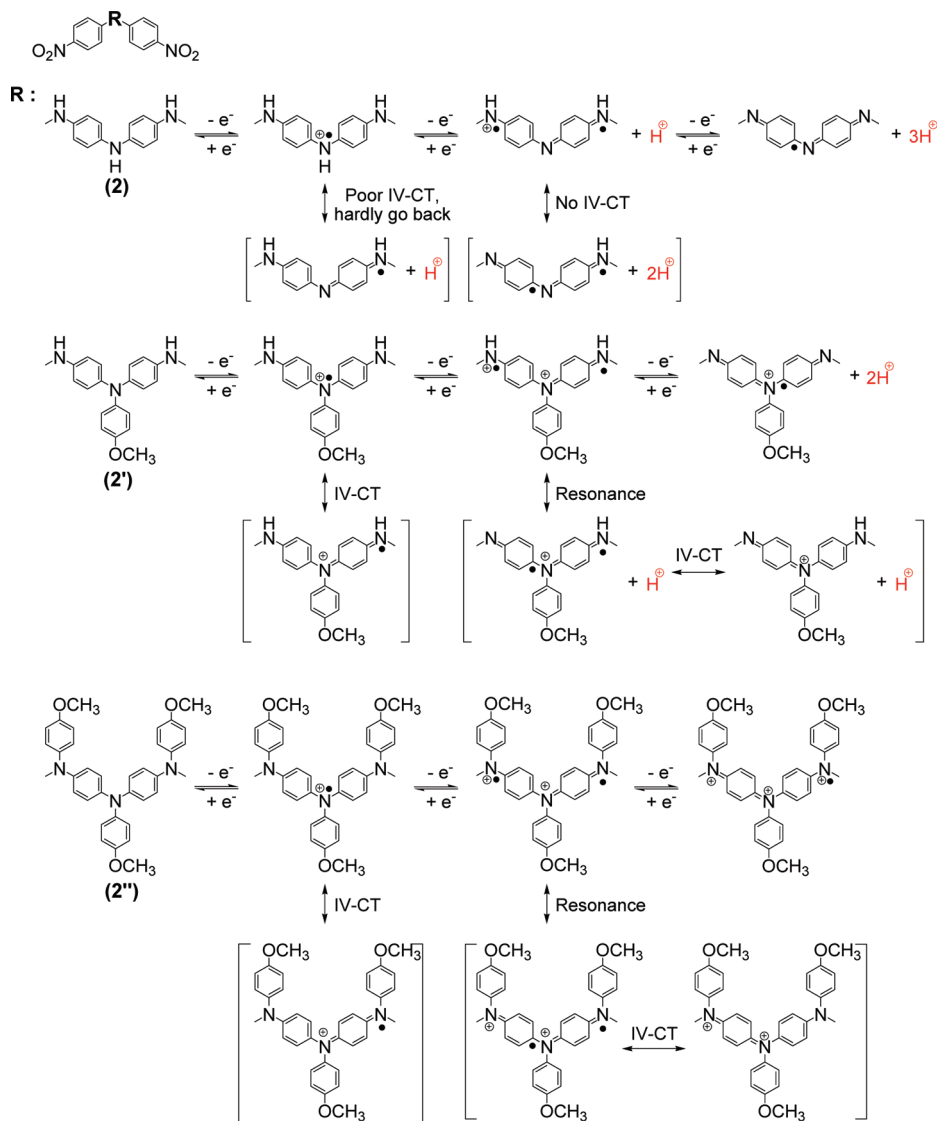
favorably with the Nernstian value of 59.1 mV for a one-electron process.

Spectroelectrochemistry and Electrochromic Properties. Spectroelectrochemical experiments were used to evaluate the optical properties of these electrochromic materials. For the investigations, dinitro compounds **2−2″** and polyimide films were prepared in the same manner as described above, and a homemade electrochemical cell was built from a commercial ultraviolet (UV)−visible cuvette. The cell was placed in the optical path of the sample light beam in a UV−vis−NIR spectrophotometer, which allowed us to acquire electronic absorption spectra under potential control. UV−vis−NIR absorbance curves correlated to applied potentials of these dinitro compounds are presented in Figure 5. The absorption peaks at 296 and 407 nm are characteristic for the $\pi-\pi^*$ transition of the aromatic phenyl ring and charge transfer complex formation of compound **2**, respectively. It revealed a red shift from 296 to 309 nm (from compound **2** to compound **2″**), owing to increasing the conjugated length by incorporating the phenyl

ring. After one-electron oxidation, the original peak decreased with a broad band at NIR region increased gradually. The broad absorption in NIR region was the characteristic result due to IV-CT excitation between states in which the positive charge is centered at different nitrogen atoms, and the phenomenon was consistent with the classified by Robin and Day.[14] When the potential was adjusted to more positive values corresponding to the second electron oxidation, the characteristic new peak at around 650−850 nm appeared. It is worth noting that the NIR region absorbance of compound **2** decreased more obviously than others, which might be attributed to the deprotonation from these secondary amino groups thus eliminated the resonance of the dications and decreased the IV-CT absorbance. The possible resonance forms of compounds **2−2″** are proposed in Scheme 3. As the applied potentials increased to the third oxidation state, the NIR wavelength decreased. Because of the incorporation of the methoxyphenyl group at secondary amine, the cation radicals of compound **2″** could be stabilized effectively to show the
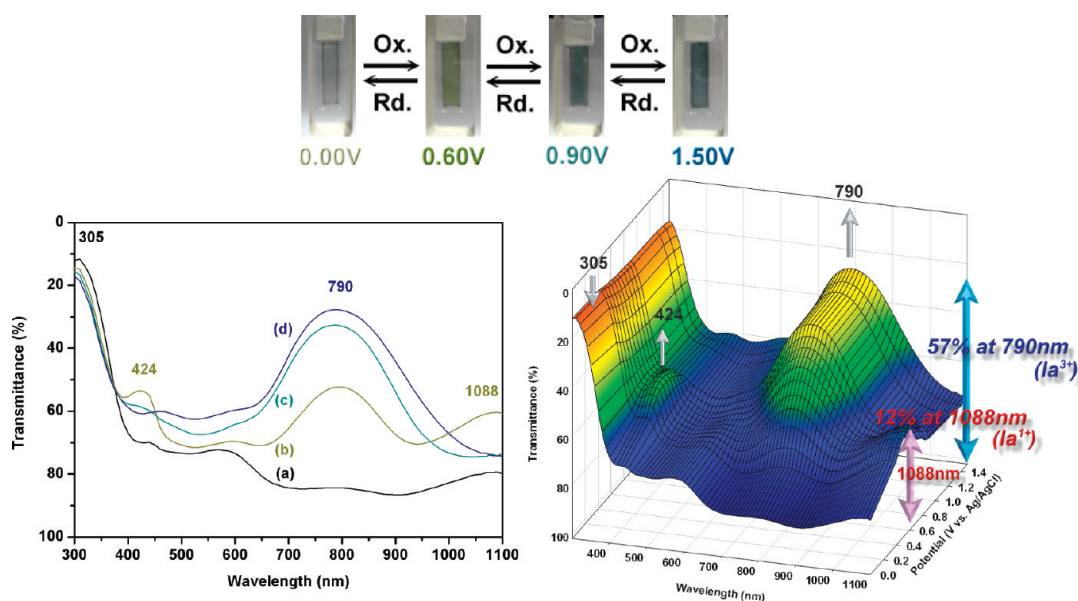
Figure 6. Electrochromic behavior (left) at applied potentials of (a) 0.00, (b) 0.60, (c) 0.90, and (d) 1.50 (V vs Ag/AgCl) and 3D spectro-electrochemical behavior (right) from 0.00 to 1.50 (V vs Ag/AgCl) of polyimide **Ia** thin film (~250 nm in thickness) on the ITO-coated glass substrate (coated area: 1.1 cm × 0.5 cm) in 0.1 M TBAP/CH$_3$CN.
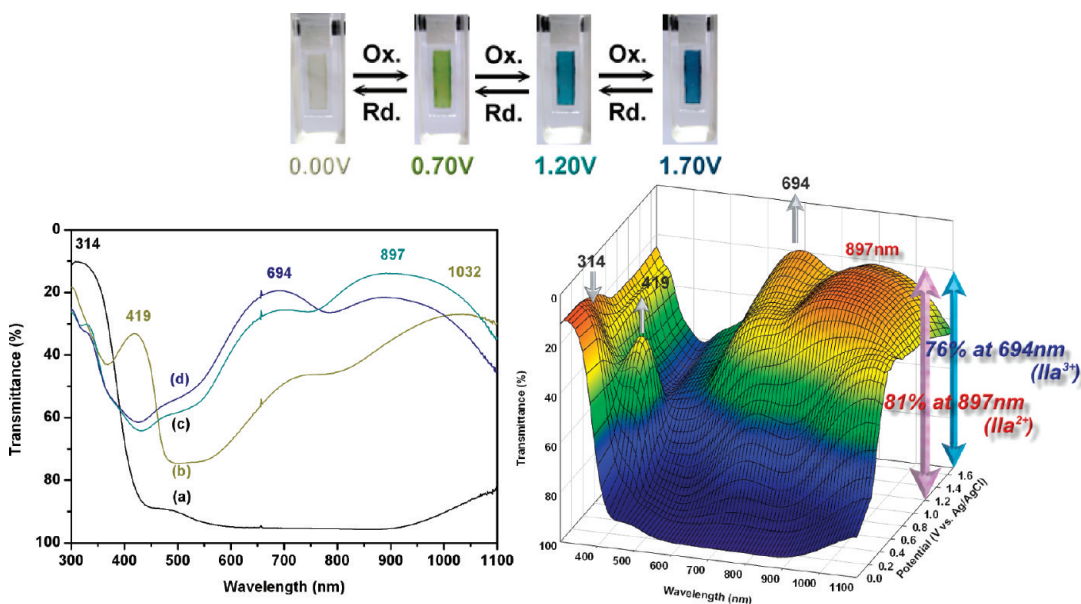

Figure 7. Electrochromic behavior (left) at applied potentials of (a) 0.00, (b) 0.70, (c) 1.20, and (d) 1.70 (V vs Ag/AgCl) and 3D spectro-electrochemical behavior (right) from 0.00 to 1.70 (V vs Ag/AgCl) of polyimide **IIa** thin film (~250 nm in thickness) on the ITO-coated glass substrate (coated area: 1.1 cm × 0.5 cm) in 0.1 M TBAP/CH$_3$CN.

highest reversibility of 100, 98, and 97% at the first, second, and third oxidation stages, respectively.

The typical spectroelectrochemistry and three-dimentional % transmittance-wavelength-applied potential correlations of poly-imide **Ia**−**IIIa** films are presented in Figures 6−8, respectively. The **Ia** film exhibited strong absorption at around 305 nm, characteristic of the $\pi-\pi^*$ transition of the aromatic phenyl rings in the neutral form (0.00 V) with a color of pale green in the visible region. Upon oxidation (increasing applied voltage from 0.00 to 0.60 V), the intensity of the absorption peak at

305 nm gradually decreased while a new peak at 424 nm and a broad IV-CT band centered around 1088 nm in the NIR region gradually increased due to the formation of a monocation radical of the diphenylamine moiety. As mentioned before, the broad absorption in NIR region was the result due to IV-CT excitation between states in which the positive charge is centered at different nitrogen atoms. As the more anodic potential to 0.90 V corresponding to **Ia**$^{2+}$, the absorption bands (305, 424, and 1088 nm) decreased gradually with a new broad band centered at around 790 nm. Similar to the compound **2**, the
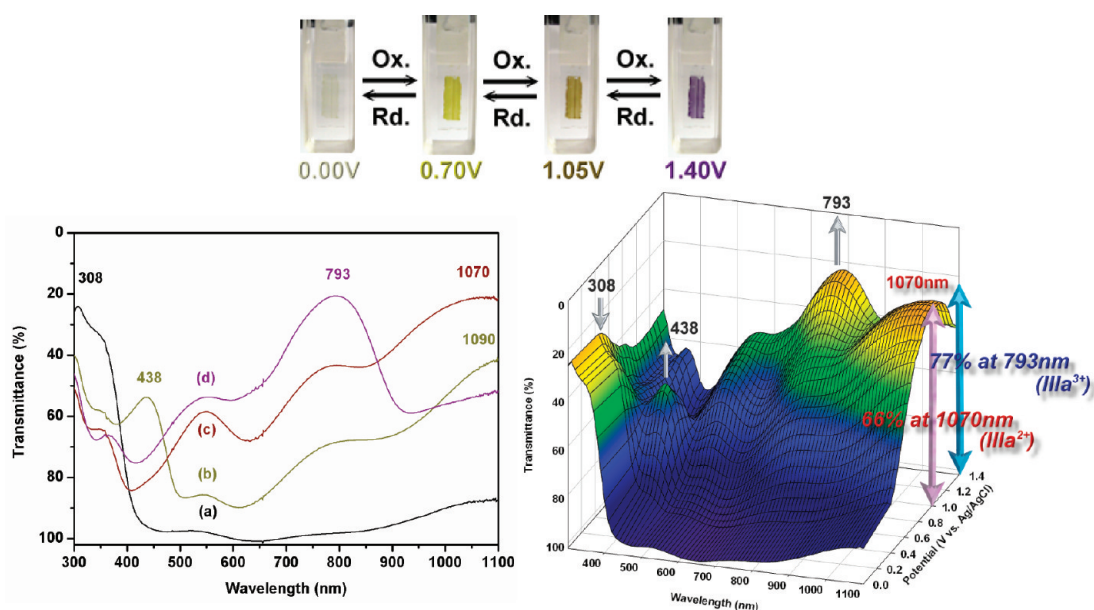
Figure 8. Electrochromic behavior (left) at applied potentials of (a) 0.00, (b) 0.70, (c) 1.05, and (d) 1.40 (V vs Ag/AgCl) and 3D spectroelectrochemical behavior (right) from 0.00 to 1.40 (V vs Ag/AgCl) of polyimide **IIIa** thin film (∼200 nm in thickness) on the ITO-coated glass substrate (coated area: 1.1 cm × 0.5 cm) in 0.1 M TBAP/CH$_3$CN.

disappearance of NIR absorption band could be attributable to the formation of imine structure by the further oxidation of second electroactive nitrogen atom. Further increasing potential up to 1.50 V corresponding to **Ia**$^{3+}$, the characteristic absorbance at 790 nm increased slightly. From the results shown in Figure 6, the polyimide **Ia** film could be switched from a pale green neutral state (0.00 V) to the light green first oxidized state (0.60 V), light bluish green second oxidized state (0.90 V), and deep bluish green fully oxidized state with a extremely low optical transmittance change ($\Delta T \%$) of 12% at 1088 nm for light green coloring at first oxidation stage and 57% at 790 nm for deep bluish green coloring at the third oxidation stage.

The spectroelectrochemical behavior of the **IIa** film is shown in Figure 7. In the neutral form, the polymer film with high transparency and pale yellowish exhibited a strong band at 314 nm, characteristic of triarylamine absorption. Upon oxidation of the **IIa** film (increasing electrode potential from 0.00 to 0.70 V), the intensity of the absorption band at 314 nm gradually decreased, whereas new peaks at 419 and 1032 nm appeared in the visible and NIR regions, respectively, relating to formation of a stable monocation radical **IIa**$^{1+}$. Further oxidation of **IIa**$^{1+}$ species to the formation of **IIa**$^{2+}$, the absorption bands (314 and 419 nm) decreased gradually with new broad band centered at around 897 nm, and the IV-CT band in the NIR region decreased slightly. When the applied potential was increased to fully oxidized form corresponding to **IIa**$^{3+}$, the absorption band at 897 nm decreased slightly with the increasing absorption intensity at around 694 nm. The polyimide **IIa** film at various potentials was associated with strong color changes switching from a pale yellow at neutral state to green at semi-oxidized states and then to dark blue at fully oxidized state. In addition, the polymer **IIa** showed good contrast both in the visible and NIR regions with a high optical transmittance change ($\Delta T \%$) of 81% at 897 nm for bluish green coloring at second oxidation stage and 76% at 694 nm for blue coloring at the third oxidation stage, respectively.

The electrochromic results of the **IIIa** film upon oxidation (p-doping) are depicted in Figure 8. The polymer film exhibited a strong absorption at around 308 nm at the neutral form with high transparency in the visible region. Similar to the process mentioned above, upon oxidation of the **IIIa** film (from 0.00 to 0.70 V), the absorbance at 308 nm gradually decreased, while a new peak at 438 nm and a broad band with maximum absorption at 1090 nm in the NIR region gradually increased in intensity. As the more anodic potential to 1.05 V, the absorption bands at the 438 nm gradually decreased while IV-CT absorption broad band still increased with a slightly shift from 1090 to 1070 nm. By further applying potential up to 1.40 V, the characteristic absorbance at 793 nm increased obviously with greatly decreasing NIR absorption band could be attributed to the further oxidation of **IIIa**$^{2+}$ species to the formation of **IIIa**$^{3+}$ in the triarylamine units. Meanwhile, the color of the film changed from very pale yellowish of neutral state to the yellowish-green/lawn-green semioxidation states and purple fully oxidation state. From the inset shown in Figure 8, the polymer **IIIa** exhibited highly optical transmittance changes ($\Delta T \%$) of 66% at 1070 nm for lawn-green coloring at the second oxidation stage and 77% at 793 nm for purple coloring at third oxidation stage, respectively. The film colorations were distributed homogeneously across polymer film and survived for more than 100 redox cycles. Comparing the optical transmittance differences between these three series of polymers, the TPA-based polyimides revealed higher contrast than diphenylamine (DPA)-based polyimides.

Figure 9 shows cathodically electrochemical behaviors of these ambipolar electrochromic polyimides **IIIa** and **IIIc** films upon reduction (n-doping) scanning. The radical anion of polyimide **IIIa** which appeared at −0.75 and −1.35 V exhibited an increasing absorption between 400 and 600 nm and a strong broad absorption band with a peak at 730 nm. Meanwhile, the color of the film changed from pale yellow to red (Figure 9a). For the polyimide **IIIc**, it exhibited a strong
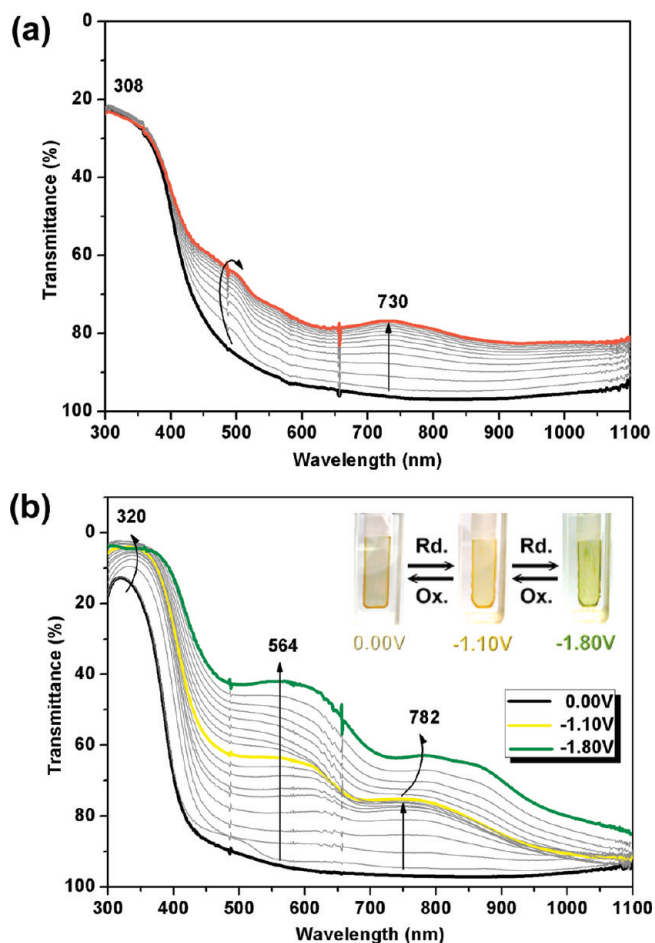
Figure 9. Optical spectra of polyimides (a) **IIIa** and (b) **IIIc** thin films (∼260 nm in thickness) on the ITO-coated glass substrate (coated area: 1.1 cm × 0.5 cm) in 0.1 M TBAP/DMF at various applied potentials versus Ag/AgCl. The inset shows the n-doping electrochromic photographic images of the film at indicated applied voltages.

absorption band at 320 nm with an increasing absorption between 400 and 650 nm due to the formation of radical anion **IIIc**[1−] (at −1.10 V). As shown in the inset of Figure 9b, the radical anion state of polyimide **IIIa** was yellow in color. Further reduction to applied potential −1.80 V resulted in the dianion state with broad absorption maxima at 564 and 782 nm, and the color of polyimide **IIIa** film turned to green in the second reduction.

Electrochromic Switching Studies. Electrochromic switching studies of these resulting polyimide films were performed to monitor the absorbance changes as a function of time at their absorption maximum and to determine the response time by stepping potential repeatedly between the neutral and oxidized states. First, structurally related PANI was investigated systematically to manifest the electrochemical and electrochromic characteristics both in the acidic and nonacidic solution, respectively, and the results are summarized in Figure S11 of the Supporting Information and Figure 10. The response time was calculated at 90% of the full switch because it is difficult to perceive any further color change with naked eye beyond this point. As depicted in Figure S11a,b, when the potential was switched between 0.00 and 0.40 V, PANI revealed response

time of 1.29 s for coloring process and 4.64 s for bleaching. When the switched potential was set between 0.00 and 0.93 V, PANI required 1.72 s for coloration and 1.80 s for bleaching. It is noteworthy that the coloring of PANI proceeded during the anodic oxidation faster than the bleaching in the reverse cathodic reduction process, which is very different from nonconjugated polymer system. This phenomenon was also described and discussed in the previous reporte.[23] The amount of extracted/injected charge (Q_r) was calculated by integration of the current density and time obtained from Figure S11c as 7.535 and 7.241 mC/cm^2 for oxidation and reduction process at the first oxidation stage, respectively, and the ratio of charge density was 96.1%. Similarly, the ratio of charge density could be obtained only 80.4% at the fully oxidation stage, indicating lower stability of PANI during the electrochemical reaction at the fully oxidation stage. Color efficiency, CE ($\eta = \delta OD/Q$), and injected charge (Q) within continuous switching steps in both acidic and nonacidic solutions were examined and summarized in Tables S4 and S5 of the Supporting Information. Comparing the first oxidation stage in these two different solvent systems, the PANI film in 1 M HCl revealed higher decay than in 0.1 M TBAP/CH$_3$CN. Although it could keep the maximum coloring absorbance but the optical contrast value declined obviously after 50 cycles, and the switching time was also much elongated (Figure 10a). This result was similar to early studies.[10] Furthermore, even the cycle time was increased from 60 to 150 s in acidic system to give more enough time to return to the original state, but the switching and bleaching time still elongated and optical contrast value decreased more obviously than before (Figure S12). In the fully oxidized state, the PANI film in 1 M HCl exhibited highly optical contrast (Figure 10b). However, the coloring efficiency decreased obviously due to the degradation of polymer film caused by oxidation under the high applied potential. In contrast, the electrochromic performance of PANI in nonacidic solution was quite unstable at the fully oxidized state. It could not bleach color to the original absorbance even only after 1 cycle, and the phenomenon might be attributed to no protons could be received from a nonacidic system (Figure 10d). Therefore, the conjugated PANI could obtain protons from acidic solution to return to original state after oxidation, while it may degrade gradually due to the acidic aqueous solution.

The typical switching results for these representative films of polyimides **Ia**, **IIa**, and **IIIa** are shown in Figures S13 and S14 of the Supporting Information and Figure 11, respectively. Among the three series, the polyimide **IIIa** (Figure 11) showed the fastest response time than others. When the applied potential was adjusted to the first oxidation stage from 0.00 to 0.70 V, the coloring and bleaching time were less than 5 and 2 s, respectively, with 99% of the ratio of the charge density. While the switched potential was set between 0.00 and 0.94 V, the polyimide **IIIa** thin film required almost the same times for coloration and bleaching with 96% of the ratio of the charge density. The electrochromic stability of the polyimide **Ia**, **IIa**, and **IIIa** films was also determined by measuring the optical change as a function of the number of switching cycles (Figures 12−14). The coloration efficiency at different switching steps is summarized in Tables 3 and 4. After continuous 100 cyclic scanning at the first oxidation stage, the polyimide **Ia** film reduced electroactivity rapidly
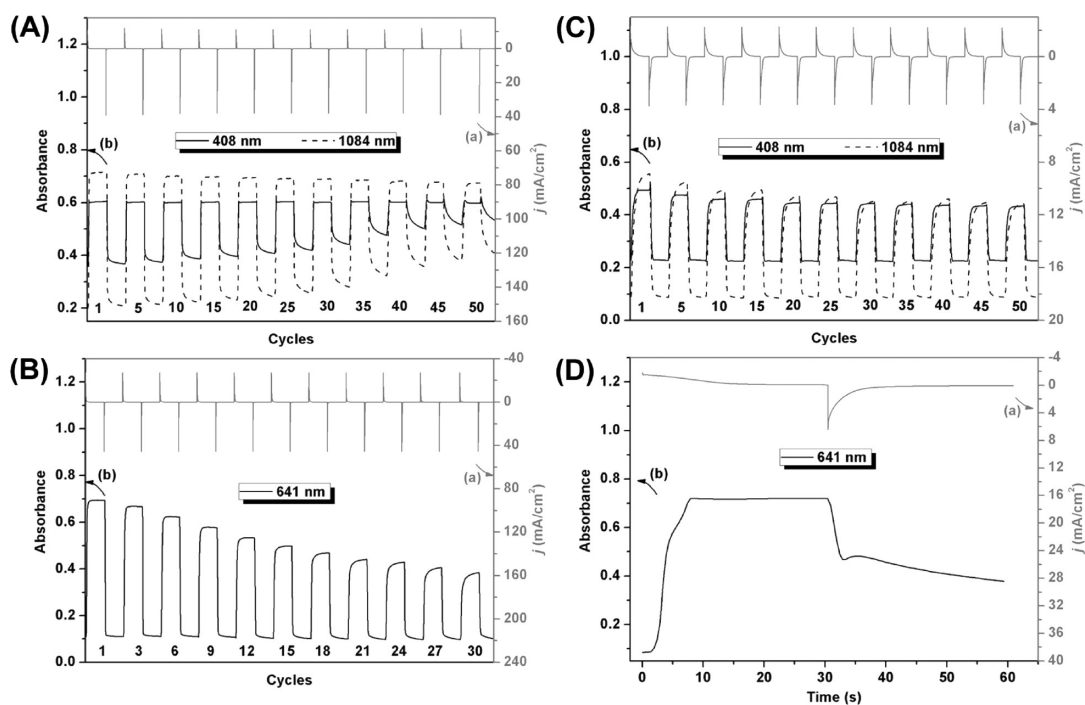
Figure 10. Electrochromic switching between (A) −0.2 and 0.40 V and (B) −0.2 and 1.00 V (vs Ag/AgCl) of PANI film (∼770 nm in thickness) deposited on the ITO-coated glass substrate (deposited area: 1.2 cm × 0.6 cm) in 1.0 M HCl with a cycle time of 60 s. (C) −0.2 and 0.70 V and (D) −0.2 and 1.50 V (vs Ag/AgCl) of PANI film (∼700 nm in thickness) in 0.1 M TBAP/CH$_3$CN with a cycle time of 60 s. (a) Current consumption and (b) absorbance change monitored at the given wavelength.

(Figure 12a). On the contrary, the polymer **IIIa** was found to exhibit high CE up to 171 cm^2/C at 1090 nm and to retain their electroactivity after switching 100 times between 0.00 and 0.70 V with only slightly decay of 0.58% (Figure 14a and Table 3). As the applied switching potential increased to the second oxidation stage, the polymer **IIIa** still revealed good electrochromic characteristics, and a higher CE (168 cm^2/C at 1070 nm) could be obtained with only 1.19% decay of its electroactivity after 30 cycles (Figure 14b and Table 4). These results were also consistent with the above-mentioned assumption that the incorporating 4-methoxyphenyl moieties into the nitrogen atom of amino groups could effectively stabilize the cation radicals by the additional extra resonance routes.

CONCLUSIONS

Three series of novel ambipolar electrochromic aromatic polyimides containing electroactive aniline-based diphenylamine or triphenylamine derivatives were prepared from the diamine monomers 4,4′-bis[(4-aminophenyl)amino]diphenylamine, 4,4′-bis[(4-aminophenyl)amino]-4″-methoxytriphenylamine, and 4,4′-bis[4-aminophenyl(4-methoxyphenyl)amino]-4″-methoxytriphenylamine, with various tetracarboxylic dianhydrides. Introduction of the methoxy-substituted phenyl groups into the nitrogen atom position not only stabilized its radical cations but also enhanced the solubility of the resulting polyimides. In addition to the excellent thermal stability, these polymers also revealed valuable electrochromic characteristics in both visible and NIR regions. The series of conjugated DPA-based polyimides could not effectively stabilize the cationic radicals of oxidized form comparing to the corresponding nonconjugated TPA-based polymers due to lack of

the extra phenyl rings as the additional routes for resonance. Furthermore, the lower electrochemical stability of the DPA-based polyimides **I** than the TPA-based polyimides **III** also could be attributed to the unrecoverable protons in the amino groups after removed in the nonacidic solution.

EXPERIMENTAL SECTION

Materials. 4,4′-Diaminodiphenylamine[19] (**1**, mp = 158−160 °C) was purified by a previously reported procedure. 4,4′-Diamino-4″-methoxytriphenylamine[12b,24,25] (**1′**, mp = 150−152 °C) and 4,4′-bis[4-aminophenyl(4-methoxyphenyl)amino]-4″-methoxytriphenylamine[18] (**3″**) were synthesized according to a previously reported procedure. Synthesis and characterization data of compounds 4,4′-bis[(4-nitrophenyl)amino]diphenylamine (**2**), 4,4′-bis[(4-aminophenyl)amino]diphenylamine (**3**), 4,4′-bis[(4-nitrophenyl)amino]-4″-methoxytriphenylamine (**2′**), and 4,4′-bis[(4-aminophenyl)amino]-4″-methoxytriphenylamine (**3′**) are included in the Supporting Information (Figures S1−S4). Commercially available aromatic tetracarboxylic dianhydrides such as 3,3′,4,4′-diphenylsulfonetetracarboxylic dianhydride (DSDA) (**4a**) (TCI), 2,2-bis(3,4-dicarboxyphenyl)hexafluoropropane dianhydride (6FDA) (**4b**) (Chriskev), and 3,3′,4,4′-biphenyltetracarboxylic diandydride (BPDA) (**4c**) (Oxychem) were purified by vacuum sublimation. Commercially obtained anhydrous calcium chloride (CaCl$_2$) was dried under vacuum at 180 °C for 8 h. Tetrabutylammonium perchlorate (TBAP) (Acros) was recrystallized twice by ethyl acetate under a nitrogen atmosphere and then dried *in vacuo* prior to use. All other reagents were used as received from commercial sources.

Polymer Synthesis. *I−II Series of Polyimides.* The synthesis of polyimide **IIa** was used as an example to illustrate the general synthetic route used to produce the **II** series of polyimides (**IIa−IIb**). The solution of 0.24 g (0.50 mmol) of diamine **3′** in 2.3 mL of DMAc was mechanically stirred at room temperature. Until the diamine monomer
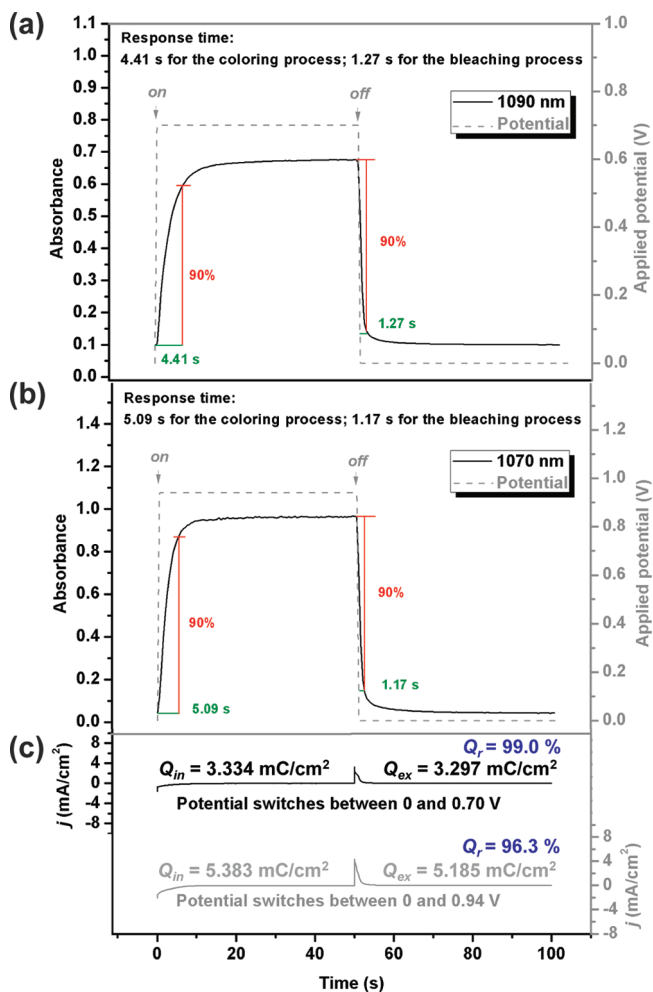
Figure 11. Calculation of optical response time at (a) 1090 nm and (b) 1070 nm at the applied potential, and (c) current−time curves of polyimide **IIIa** thin film (∼300 nm in thickness) coated on the ITO-coated glass substrate (coated area: 1.1 cm × 0.5 cm) in 0.1 M TBAP/CH$_3$CN.
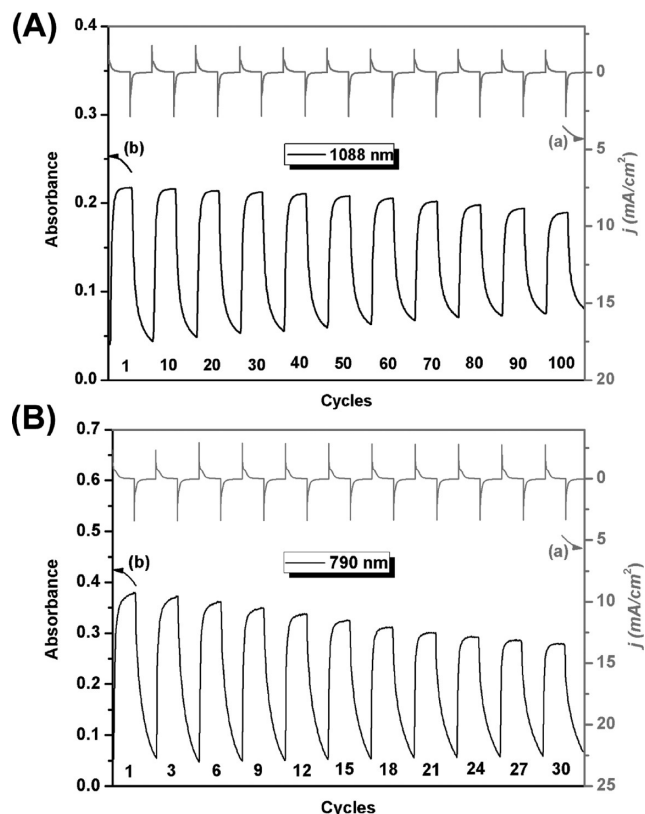

Figure 12. Electrochromic switching between (A) 0 and 0.58 V and (B) 0 and 0.83 V (vs Ag/AgCl) of polyimide **Ia** thin film (∼260 nm in thickness) on the ITO-coated glass substrate (coated area: 1.1 cm × 0.5 cm) in 0.1 M TBAP/CH$_3$CN with a cycle time of 60 s. (a) Current consumption and (b) absorbance change monitored at the given wavelength.

dissolved completely, using liquid nitrogen with an ice bath to freeze the solution. And then, 0.18 g (0.50 mmol) of dianhydride DSDA (**4a**) was added in one portion (15 wt % solid content). The mixture was mechanically stirred and kept at low temperature (ca. −10 °C) for about 2.5 h to yield a viscous poly(amic acid) solution. The poly(amic acid) was subsequently converted to polyimide **IIa** via a chemical imidization process by addition of pyridine 0.25 mL (3.10 mmol) and acetic anhydride 0.29 mL (3.10 mmol), and the mixture was heated at 120 °C for 2 h to effect complete imidization. The resulting polymer solution was poured into 100 mL of methanol, giving a yellowish brown precipitate, which was washed thoroughly with methanol, and collected by filtration. For **I** series of polyimides (**Ia**−**Ib**), it just only changed the solvent as NMP and added the salts (CaCl$_2$) in the procedure to prevent the side reaction and disrupt the hydrogen-bonding interaction. The inherent viscosity and weight-average molecular weights (M_w) of obtained polyimide **IIa** were 1.30 dL/g (measured at a concentration of 0.5 g/dL in NMP at 30 °C) and 122 000 Da, respectively. The FT-IR spectrum of **IIa** (film) exhibited characteristic imide absorption bands at around 1779 (asymmetrical C═O), 1721 (symmetrical C═O), 1382 (C−N), and 739 cm^{-1} (imide ring deformation). ^{1}H NMR (500 MHz, DMSO-d_6, δ, ppm): 8.56 (s, 4H, H$_i$ + H$_h$), 8.25 (s, 2H, −NH), 8.13 (s, 2H, H$_g$), 7.16 (s, 4H, H$_f$), 7.04 (s, 8H,

H$_d$ + H$_e$), 6.94 (s, 2H, H$_b$), 6.87 (s, 6H, H$_a$ + H$_c$), 3.69 (s, 3H, −OCHH$_3$). ^{13}C NMR (125 MHz, DMSO-d_6, δ, ppm): 166.1 (C^{20}), 166.0 (C^{19}), 155.0 (C^{12}), 145.3 (C^8), 144.7 (C^4), 141.8 (C^5), 141.0 (C^9), 137.0 (C^1), 136.3 (C^{16}), 134.3 (C^{15}), 133.3 (C^{13}), 128.4 (C^2), 125.4 (C^{10}), 124.9 (C^{14}), 124.0 (C^7), 122.7 (C^{17}), 122.0 (C^{18}), 119.8 (C^3), 115.2 (C^6), 114.9 (C^{11}), 55.3 (−OCH$_3$). Anal. Calcd (%) for C$_{47}$H$_{31}$N$_5$O$_7$S (809.84): C, 69.71%; H, 3.86%; N, 8.65%. Found: C, 67.13%; H, 4.18%; N, 8.82%.

***III** Series of Polyimides.* Furthermore, in addition to **IIIa** and **IIIb**, the diamine **3″** was chosen to react with BPDA (**4c**) to obtain the polyimide **IIIc** which would reveal more interesting muti-electrochromism behaviors during both p- and n-doping processes. The synthesis of polyimide **IIIa** was used as an example to illustrate the general synthetic route used to produce the **III** series of polyimides (**IIIa**−**IIIc**). Into a 50 mL round-bottom flask were added 0.35 g (0.50 mmo) of diamine **3″**, 0.18 g (0.50 mmol) of dianhydride DSDA (**4a**), 0.12 mL of isoquinoline, and 2 mL of *m*-cresol. The reaction mixture was stirred at room temperature in a nitrogen atmosphere for 5 h. Then, the reaction temperature was increased to 185 °C for 15 h. After the imidization reaction, the mixture was cooled to room temperature; the viscous polymer solution then was poured slowly into 100 mL of methanol with stirring. A yellowish brown precipitate was washed thoroughly with hot methanol, collected by filtration, and dried in vacuum at 80 °C for 15 h. The inherent viscosity and weight-average molecular weights (M_w) of obtained polyimide **IIIa** was 0.33 dL/g (measured at a concentration of 0.5 g/dL in NMP at 30 °C) and 66 000 Da, respectively. The FT-IR spectrum of **IIIa** (film) exhibited characteristic imide absorption bands
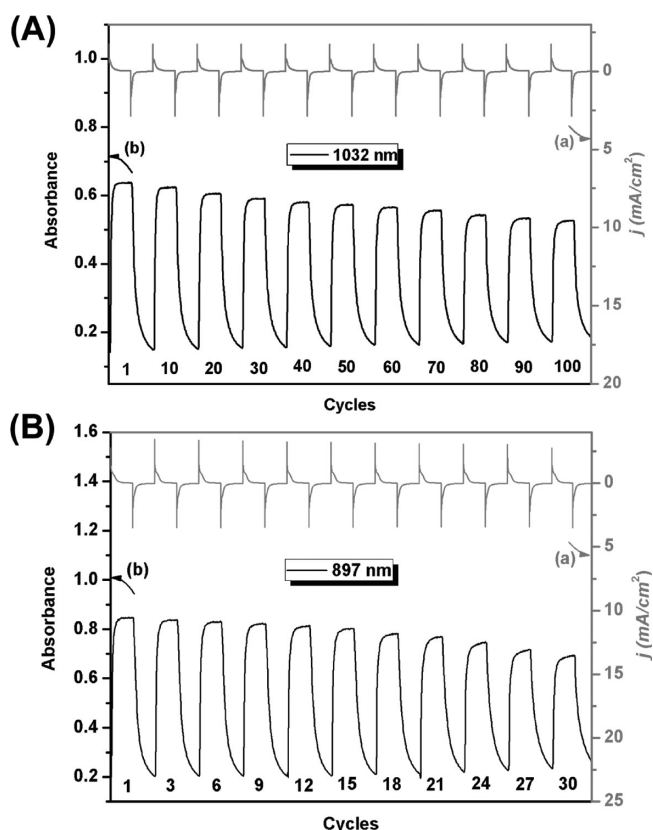
Figure 13. Electrochromic switching between (A) 0 and 0.71 V and (B) 0 and 1.10 V (vs Ag/AgCl) of polyimide **IIa** thin film (~300 nm in thickness) on the ITO-coated glass substrate (coated area: 1.1 cm × 0.5 cm) in 0.1 M TBAP/CH$_3$CN with a cycle time of 60 s. (a) Current consumption and (b) absorbance change monitored at the given wavelength.
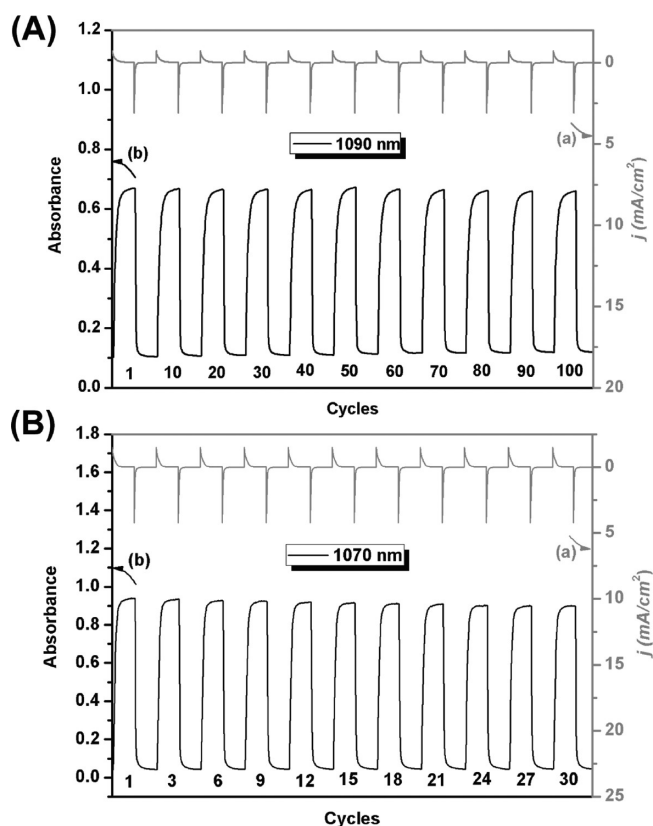

Figure 14. Electrochromic switching between (A) 0 and 0.70 V and (B) 0 and 0.94 V (vs Ag/AgCl) of polyimide **IIIa** thin film (~300 nm in thickness) on the ITO-coated glass substrate (coated area: 1.1 cm × 0.5 cm) in 0.1 M TBAP/CH$_3$CN with a cycle time of 60 s. (a) Current consumption and (b) absorbance change monitored at the given wavelength.

at around 1783 (asymmetrical C=O), 1720 (symmetrical C=O), 1380 (C−N), and 724 cm^{-1} (imide ring deformation). Anal. Calcd (%) for C$_{61}$H$_{43}$N$_5$O$_9$S (1022.09): C, 71.68%; H, 4.24%; N, 6.85%. Found: C, 71.40%; H, 4.61%; N, 6.40%.

Preparation of the Polyimide Films. A solution of the polymer was made by dissolving about 0.2 g of the polyimide sample in 6 mL of NMP. The homogeneous solution was poured into a 5 cm glass Petri dish, which was heated in oven at 80 °C for 5 h to remove most of the solvent; then the semidried film was further dried *in vacuo* at 160 °C for 10 h. The obtained films were about 40−90 μm thick and were used for solubility tests and thermal analyses.

Measurements. Fourier transform infrared (FT-IR) spectra were recorded on a PerkinElmer Spectrum 100 Model FT-IR spectrometer. Elemental analyses were run in a Heraeus VarioEL-III CHNS elemental analyzer. ^{1}H and ^{13}C NMR spectra were measured on a Bruker AVANCE-500 FT-NMR using tetramethylsilane as the internal standard, and peak multiplicity was reported as follows: s, singlet; d, doublet. The inherent viscosities were determined at 0.5 g/dL concentration using Tamson TV-2000 viscometer at 30 °C. Gel permeation chromatographic (GPC) analysis was carried out on a Waters chromatography unit interfaced with a Waters 2410 refractive index detector. Two Waters 5 μm Styragel HR-2 and HR-4 columns (7.8 mm i.d. × 300 mm) were connected in series with NMP as the eluent at a flow rate of 0.5 mL/min at 40 °C and were calibrated with polystyrene standards. Thermogravimetric analysis (TGA) was conducted with a PerkinElmer Pyris 1 TGA. Experiments were carried out on approximately 6−8 mg film samples

heated in flowing nitrogen or air (flow rate = 20 cm^3/min) at a heating rate of 20 °C/min. Thermal mechanical analysis (TMA) was conducted with a TA Instruments TMA Q400. The TMA experiments were conducted from 40 to 400 °C at a scan rate of 10 °C/min with a film/fiber probe under an applied constant load of 5 mN. Electrochemistry was performed with a CH Instruments 611B electrochemical analyzer. Voltammograms are presented with the positive potential pointing to the left and with increasing anodic currents pointing downward. Cyclic voltammetry (CV) was conducted with the use of a three-electrode cell in which ITO (polymer films area about 0.5 cm × 1.1 cm) was used as a working electrode. A platinum wire was used as an auxiliary electrode. All cell potentials were taken by using a homemade Ag/AgCl, KCl (sat.) reference electrode. Spectroelectrochemical experiments were carried out in a cell built from a 1 cm commercial UV−vis cuvette using a Hewlett-Packard 8453 UV−vis diode array spectrophotometer and a Hitachi U-4100 UV−vis−NIR spectrophotometer. The ITO-coated glass slide was used as the working electrode, a platinum wire as the counter electrode, and a Ag/AgCl cell as the reference electrode. CE (η) determines the amount of optical density change (δOD) at a specific absorption wavelength induced as a function of the extracted/injected charge (Q$_r$; also termed as electroactivity) which is determined from the *in situ* experiments. CE is given by the equation $\eta = \delta OD/Q = \log[T_b/T_c]/Q$, where η (cm^2/C) is the coloration efficiency at a given wavelength, Q is the injected charge, and T_b and T_c are the bleached and colored transmittance values,

Table 3. Optical and Electrochemical Data Collected for Coloration Efficiency Measurements of Polyimide Ia–IIIa

cycling times[a]	δOD_{1088}[b] Ia	δOD_{1032}[b] IIa	δOD_{1090}[b] IIIa	Q (mC/cm²)[c] Ia	IIa	IIIa	η (cm²/C)[d] Ia	IIa	IIIa	decay (%)[e] Ia	IIa	IIIa
1	0.176	0.497	0.571	4.329	4.504	3.334	41	110	171	0	0	0
10	0.165	0.489	0.571	4.328	4.503	3.334	38	109	171	7.31	0.91	0
20	0.163	0.468	0.571	4.325	4.501	3.334	37	104	171	9.76	5.45	0
30	0.151	0.455	0.571	4.325	4.501	3.334	35	101	171	14.6	8.18	0
40	0.147	0.444	0.571	4.326	4.501	3.334	34	99	171	17.1	10.0	0
50	0.143	0.432	0.571	4.324	4.501	3.334	33	96	171	19.5	12.7	0
60	0.134	0.423	0.571	4.323	4.498	3.334	31	94	171	24.4	14.5	0
70	0.127	0.416	0.570	4.323	4.498	3.333	29	92	171	29.3	16.4	0
80	0.121	0.404	0.570	4.321	4.498	3.334	28	90	171	31.7	18.2	0
90	0.117	0.397	0.568	4.320	4.497	3.334	27	88	170	34.1	20.0	0.58
100	0.106	0.388	0.568	4.320	4.497	3.334	24	86	170	41.5	21.8	0.58

[a] Switching between 0 and 0.58 V for **Ia**, 0 and 0.71 V for **IIa**, and 0 and 0.70 V for **IIIa** (V vs Ag/AgCl). [b] Optical density change at the given wavelength. [c] Ejected charge, determined from the in situ experiments. [d] Coloration efficiency is derived from the equation $\eta = \delta OD/Q$. [e] Decay of coloration efficiency after cyclic scans.

Table 4. Optical and Electrochemical Data Collected for Coloration Efficiency Measurements of Polyimides Ia–IIIa

cycling times[a]	δOD_{790}[b] Ia	δOD_{897}[b] IIa	δOD_{1070}[b] IIIa	Q (mC/cm²)[c] Ia	IIa	IIIa	η (cm²/C)[d] Ia	IIa	IIIa	decay (%)[e] Ia	IIa	IIIa
1	0.331	0.649	0.898	6.703	7.645	5.383	49	85	168	0	0	0
3	0.323	0.639	0.898	6.703	7.644	5.383	48	84	168	2.04	1.18	0
6	0.309	0.628	0.897	6.701	7.644	5.382	46	82	167	6.12	3.53	0.59
9	0.298	0.623	0.897	6.701	7.641	5.382	44	82	167	10.2	3.53	0.59
12	0.288	0.613	0.897	6.698	7.641	5.382	43	80	167	12.2	5.88	0.59
15	0.267	0.604	0.896	6.698	7.641	5.383	40	79	166	18.4	7.06	1.19
18	0.256	0.582	0.894	6.701	7.637	5.383	38	76	166	22.5	10.6	1.19
21	0.245	0.569	0.894	6.698	7.636	5.382	37	75	166	24.5	11.8	1.19
24	0.234	0.548	0.894	6.699	7.633	5.382	35	72	166	28.6	15.3	1.19
27	0.223	0.521	0.893	6.696	7.632	5.383	33	68	166	32.7	20.0	1.19
30	0.201	0.490	0.893	6.687	7.632	5.381	30	64	166	38.8	24.7	1.19

[a] Switching between 0 and 0.83 V for **Ia**, 0 and 1.10 V for **IIa**, and 0 and 0.94 V for **IIIa** (V vs Ag/AgCl). [b] Optical density change at the given wavelength. [c] Ejected charge, determined from the in situ experiments. [d] Coloration efficiency is derived from the equation $\eta = \delta OD/Q$. [e] Decay of coloration efficiency after cyclic scans.

respectively. The thickness of the polyimide thin films was measured by alpha-step profilometer (Kosaka Lab., Surfcorder ET3000, Japan).

■ ASSOCIATED CONTENT

ⓢ **Supporting Information.** Synthesis of compounds; table: inherent viscosity, molecular weights, solubility behavior, and thermal properties of polyimides **I–III**; optical and electrochemical data of **PANI**; figure: IR and NMR of cmpounds and polyimide, TGA and TMA traces of polyimides, CV, absorption spectra and electrochromic switching of the PANI, optical response time of PANI, **Ia**, and **IIa**; scheme: postulated redox chemistry of PANI in acid electrolytes. This material is available free of charge via the Internet at http://pubs.acs.org.

■ AUTHOR INFORMATION

Corresponding Author
*E-mail: gsliou@ntu.edu.tw.

■ REFERENCES

(1) Monk, P. M. S.; Mortimer, R. J.; Rosseinsky, D. R. *Electrochromism and Electrochromic Devices*; Cambridge University Press: New York, 2007.

(2) (a) Trevedi, D. C. Conductive Polymers: Synthesis and Electrical Properties. In *Handbook of Organic Conductive Molecules and Polymers*; Nalwa, H. S., Ed.; Wiley: New York, 1997; Vol. 2. (b) Wei, Z.; Faul, C. F. J. *Macromol. Rapid Commun.* **2008**, *29*, 280.

(3) (a) Lu, F. L.; Wudl, F.; Nowak, M.; Heeger, A. J. *J. Am. Chem. Soc.* **1986**, *108*, 8311. (b) Wei, Y.; Yang, C.; Ding, T. *Tetrahedron Lett.* **1996**, *37*, 731. (c) Wei, Y.; Yang, C.; Wei, G.; Feng, G. *Synth. Met.* **1997**, *84*, 289. (d) Zhang, W. J.; Feng, J.; MacDiarmid, A. G.; Epstein, A. J. *Synth. Met.* **1997**, *84*, 119. (e) Rebourt, E.; Joule, J. A.; Monkman, A. P. *Synth. Met.* **1997**, *84*, 65. (f) Sadighi, J. P.; Singer, R. A.; Buchwald, S. L. *J. Am. Chem. Soc.* **1998**, *120*, 4960. (g) Gao, J.; Zhang, W.; Li, K.; Wang, C.; Wu, Z.; Ji, Y. *Macromol. Rapid Commun.* **1999**, *20*, 463. (h) Gao, J.; Li, K.; Zhang, W.; Wang, C.; Wu, Z.; Ji, Y.; Zhou, Y. *Macromol. Rapid Commun.* **1999**, *20*, 560. (i) Wang, W.; MacDiarmid, A. G. *Synth. Met.* **2002**, *129*, 199. (j) Różalska, I.; Kułyk, P.; Kulszewicz-Bajer, I. *New J. Chem.* **2004**, *28*, 1235. (k) Chen, L.; Yu, Y.; Mao, H.; Lu, X.; Zhang, W.; Wei, Y. *Synth. Met.* **2005**, *149*, 129. (l) Chen, L.; Yu, Y.; Mao, H.; Lu, X.; Zhang, W.; Wei, Y. *Mater. Lett.* **2005**, *59*, 2446.

(4) He, J.; Chen, F.; Lindsay, S. *Appl. Phys. Lett.* **2007**, *90*, 072112.

(5) (a) Gao, B. J.; Liu, D. G.; Sansiňena, J. M.; Wang, H. L. *Adv. Funct. Mater.* **2004**, *14*, 537. (b) Chao, D.; Lu, X.; Chen, J.; Liu, X.; Zhang, W.; Wei, Y. *Polymer* **2006**, *47*, 2643. (c) Chao, D.; Lu, X.; Chen, J.; Zhao, X.; Wang, L.; Zhang, W.; Wei, Y. *J. Polym. Sci., Part A: Polym. Chem.* **2006**, *44*, 477. (d) Zhang, J.; Chao, D.; Cui, L.; Liu, X.; Zhang, W. *Macromol. Chem. Phys.* **2009**, *210*, 1739. (e) Cui, L.; Chao, D.; Zhang, J.; Mao, H.; Li, Y.; Wang, C. *Synth. Met.* **2010**, *160*, 400.

(6) (a) Wang, Z. Y.; Yang, C.; Gao, J. P.; Lin, J.; Meng, X. S. *Macromolecules* **1998**, *31*, 2702. (b) Lu, W.; Meng, X. S.; Wang, Z. Y. *J. Polym. Sci., Part A: Polym. Chem.* **1999**, *37*, 4295. (c) Huang, K. Y.; Jhuo, Y. S.; Wu, P. S.; Lin, C. H.; Yu, Y. H.; Yeh, J. M. *Eur. Polym. J.* **2009**, *45*, 485. (d) Chao, D.; Zhang, J.; Liu, X.; Lu, X.; Wang, C.; Zhang, W.; Wei, Y. *Polymer* **2010**, *51*, 4518.

(7) (a) Yang, X.; Jiang, Y.; Zhao, T.; Yu, Y. *J. Appl. Polym. Sci.* **2006**, *102*, 222. (b) Huang, K. Y.; Shiu, C. L.; Wu, P. S.; Wei, Y.; Yeh, J. M.; Li, W. T. *Electrochim. Acta* **2009**, *54*, 5400.

(8) Hung, W. I.; Hung, C. B.; Chang, Y. H.; Dai, J. K.; Li, Y.; He, H.; Chen, S. W.; Huang, T. C.; Wei, Y.; Jia, X. R.; Yeh, J. M. *J. Mater. Chem.* **2011**, *21*, 4581.

(9) (a) Buga, K.; Majkowska, A.; Pokrop, R.; Zagorska, M.; Djurado, D.; Pron, A.; Oddou, J. L.; Lefrant, S. *Chem. Mater.* **2005**, *17*, 5754. (b) Zhang, Q. S.; Yan, Y. H.; Li, S. P.; Feng, T. *Biomed. Mater.* **2009**, *4*, 035008. (c) Guo, B.; Wistrand, A. F.; Albertsson, A. C. *Biomacromolecules* **2010**, *11*, 855.

(10) Zhao, L.; Zhao, L.; Xu, Y.; Qiu, T.; Zhi, L.; Shi, G. *Electrochim. Acta* **2009**, *55*, 491.

(11) Amb, C. M.; Dyer, A. L.; Reynolds, J. R. *Chem. Mater.* **2011**, *23*, 397.

(12) (a) Seo, E. T.; Nelson, R. F.; Fritsch, J. M.; Marcoux, L. S.; Leedy, D. W.; Adams, R. N. *J. Am. Chem. Soc.* **1966**, *88*, 3498. (b) Nelson, R. F.; Adams, R. N. *J. Am. Chem. Soc.* **1968**, *90*, 3925.

(13) (a) Ito, A.; Ino, H.; Tanaka, K.; Kanemoto, K.; Kato, T. *J. Org. Chem.* **2002**, *67*, 491. (b) Chiu, K. Y.; Su, T. H.; Li, J. H.; Lin, T. H.; Liou, G. S.; Cheng, S. H. *J. Electroanal. Chem.* **2005**, *575*, 95.

(14) (a) Creutz, C.; Taube, H. *J. Am. Chem. Soc.* **1973**, *95*, 1086. (b) Lambert, C.; Noll, G. *J. Am. Chem. Soc.* **1999**, *121*, 8434.

(15) Robin, M.; Day, P. *Adv. Inorg. Radiochem.* **1967**, *10*, 247.

(16) Szeghalmi, A. V.; Erdmann, M.; Engel, V.; Schmitt, M.; Amthor, S.; Kriegisch, V.; Noll, G.; Stahl, R.; Lambert, C.; Leusser, D.; Stalke, D.; Zabel, M.; Popp, J. *J. Am. Chem. Soc.* **2004**, *126*, 7834.

(17) (a) Cheng, S. H.; Hsiao, S. H.; Su, T. X.; Liou, G. S. *Macromolecules* **2005**, *38*, 307. (b) Liou, G. S.; Hsiao, S. H.; Su, T. X. *J. Mater. Chem.* **2005**, *15*, 1812. (c) Liou, G. S.; Yang, Y. L.; Su, Y. L. O. *J. Polym Sci., Part A: Polym. Chem.* **2006**, *44*, 2587. (d) Liou, G. S.; Hsiao, S. H.; Chen, H. W. *J. Mater. Chem.* **2006**, *16*, 1831. (e) Liou, G. S.; Hsiao, S. H.; Huang, N. K.; Yang, Y. L. *Macromolecules* **2006**, *39*, 5337. (f) Liou, G. S.; Chen, H. W.; Yen, H. J. *J. Polym. Sci., Part A: Polym. Chem.* **2006**, *44*, 4108. (g) Liou, G. S.; Hsiao, S. H.; Chen, W. C.; Yen, H. J. *Macromolecules* **2006**, *39*, 6036. (h) Liou, G. S.; Chang, C. W.; Huang, H. M.; Hsiao, S. H. *J. Polym. Sci., Part A: Polym. Chem.* **2007**, *45*, 2004. (i) Yen, H. J.; Liou, G. S. *J. Polym. Sci., Part A: Polym. Chem.* **2009**, *47*, 1584. (J) Yen, H. J.; Liou, G. S. *Chem. Mater.* **2009**, *21*, 4062. (k) Yen, H. J.; Guo, S. M.; Liou, G. S.; Chung, J. C.; Liu, Y. C.; Lu, Y. F.; Zeng, Y. Z. *J. Polym. Sci., Part A: Polym. Chem.* **2011**, *49*, 3805. (l) Yen, H. J.; Lin, K. Y.; Liou, G. S. *J. Mater. Chem.* **2011**, *21*, 6230. (m) Yen, H. J.; Lin, H. Y.; Liou, G. S. *Chem. Mater.* **2011**, *23*, 1874.

(18) Liou, G. S.; Lin, H. Y. *Macromolecules* **2009**, *42*, 125.

(19) Kulszewicz-Bajer, I.; Róžalska, I.; Kuryłek, M. *New J. Chem.* **2004**, *28*, 669.

(20) Huang, L. T.; Yen, H. J.; Chang, C. W.; Liou, G. S. *J. Polym. Sci., Part A: Polym. Chem.* **2010**, *48*, 4747.

(21) (a) Elizabeth, W. P.; Antonio, J. R.; Mark, S. W. *J. Phys. Chem.* **1985**, *89*, 1441. (b) Cho, J. H.; Oh, E. J.; Yo, C. H. *Bull. Korean Chem. Soc.* **1996**, *17*, 715. (c) Ansari, R.; Keivani, M. B. *E-J. Chem.* **2006**, *3*, 202.

(22) Bard, A. J.; Faulkner, L. R. *Electrochemical Methods: Fundamentals and Applications*; Wiley: New York, 2001.

(23) Malinauskas, A.; Holze, R. *Synth. Met.* **1998**, *97*, 31.

(24) Nishikata, Y.; Fukui, S.; Kakimoto, M.; Imai, Y.; Nishiyama, K.; Fujihira, M. *Thin Solid Films* **1992**, *210*, 296.

(25) Chang, C. W.; Liou, G. S.; Hsiao, S. H. *J. Mater. Chem.* **2007**, *17*, 1007.